8B.2 DETECTING CLOUD ICING CONDITIONS USING CLOUDSAT DATASETS

Michael P. Kay*[12], Chungu Lu[13], Sean Madine[13], Jennifer Luppens Mahoney[1], and Pengyuan Li[4]

[1]NOAA Earth System Research Laboratory (ESRL), Boulder, Colorado
[2]Cooperative Institute for Research in Environmental Sciences (CIRES), University of Colorado, Boulder, Colorado
[3]Cooperative Institute for Research in the Atmosphere (CIRA), Colorado State University, Fort Collins, Colorado
[4]Department of Meteorology, Ocean University of China, Qingdao, China

1. INTRODUCTION

Cloud icing is one of the meteorological conditions that influences aviation safety. Icing conditions are related to cloud dynamics and microphysical processes that promote the existence of supercooled liquid water above freezing levels inside clouds. There is no conventional meteorological observation for this field, but commercial aircraft do give icing reports (pilot reports; PIREPs) whenever they encounter such situations. Examples of nowcasts and forecasts of icing conditions include the Current Icing Potential (CIP; Bernstein et al. 2005), the Forecast Icing Potential (FIP), and Significant Weather (SigWx) charts.

Many previous studies have used various geostationary and polar-orbiting meteorological satellites to derive cloud icing information (Curry and Liu 1992; Ellrod 1996; Vivekanandan et al. 1996; Thompson et al. 1997; Smith et al. 2000; Minnis et al. 2004; Ellrod and Bailey 2007; Lee et al. 2007; Wolff et al. 2008). In particular, Ellrod and Bailey (2007) assessed aircraft icing potential and maximum icing altitudes using data from the Geostationary Operational Environmental Satellite (GOES) imager and sounder. Lee et al. (2007) studied icing nowcasting capability using CloudSat. In order to validate CIP, Wolff et al. (2008) proposed using CloudSat's cloud geometric profile data to compare cloud top heights between CIP and CloudSat.

* *Corresponding author address:* Michael P. Kay, R/GSD5, 325 Broadway, Boulder, CO 80305; email: mike.kay@noaa.gov

The recent launch of NASA A-train satellites, a series of polar orbiting satellites, aims at providing better global observations of clouds and precipitation over the Earth. The CloudSat is one of the NASA A-train satellites. Carrying a powerful cloud-profiling radar, CloudSat is designed as a new satellite-based cloud observatory, which possesses the abilities to make detailed observations of clouds from space (Stephens et al. 2002). In particular, CloudSat datasets are able to provide a direct view of clouds and cloud structures. With these datasets some microphysical properties of clouds may be deduced.

In this study, we present an algorithm for diagnosing potential icing conditions using CloudSat cloud classification data. Several case studies will be shown, demonstrating the similarities and differences of cloud icing conditions derived from CloudSat with those from aircraft observations and CIP. Additional objective intercomparison results between our algorithm and CIP will also be presented.

2. CLOUDSAT AND CLOUDSAT DATA PROCESSING

CloudSat carries a 94-GHz, nadir-pointing Cloud Profiling Radar (CPR). Because the CPR operates at millimeter wavelength, it can detect cloud particles adequately (Stephens et al. 2002). Backscatter from cloud particles is converted into radar reflectivity, which comprises the principal CloudSat dataset. The data provide a track-vertical cross-section view of cloud structure, with vertical resolution of 240 m from surface to a 30-km altitude. The horizontal footprint of

each profile is 1.1 km.

Several other CloudSat datasets that combine a subset of MODIS and AMSR-E radiance data, as well as a number of selected MODIS and CERES products specifically matched to the CloudSat radar ground track are available. In this study, we focus in particular on the CloudSat cloud classification product. The cloud classification product provides a diagnosis of the type of cloud present at each profile location within the satellite track. The detailed methodology of our use of this information will be discussed in the next section. The CloudSat data were retrieved from the CloudSat Data Processing Center located at the Colorado State University.

3. METHODOLOGY

Many studies have shown that supercooled liquid water can exist inside clouds above the freezing level (Rauber and Tokay 1991; Tabazadeh et al. 2002; Rosenfeld and Woodley 2000; Heymsfield and Miloshevich 1989, 1993). When an aircraft flies through areas where a significant amount of supercooled water exists, the supercooled water has the potential to quickly freeze on the body of the aircraft creating a significant safety concern. Owing to differences in microphysical processes as well as environmental temperatures, the location of supercooled liquid water varies tremendously throughout the global atmosphere. Furthermore, strong updrafts within developing convective clouds may also influence the locations where icing conditions may exist with supercooled water carried up to altitudes with temperatures much colder than 0°C.

Based on these studies, we have designed an algorithm, CloudSat Icing Potential (CLIP), to combine CloudSat cloud classification data with global temperature profiles produced by a global atmospheric model to provide a diagnosis of icing potential. The initial step in the algorithm is to create a series of interpolated vertical temperature profiles along the satellite track co-located with the individual profiles. We have used global temperatures from the NCAR reanalysis archive for this purpose however data from any other global data source or model could be substituted. The CloudSat cloud classification data allows for the following eight cloud types: stratocumulus (Sc), stratus (St), altocumulus (Ac), altostratus (As), cumulus (Cu), nimbostratus (Ns), deep convective, cirrus (Ci), cirrostratus (Cs), and cirrocumulus (Cc). The range of temperatures within each cloud type where supercooled liquid is likely to be found are displayed in Table 1. In all cases, supercooled liquid is not allowed at temperatures warmer than 0°C or colder than -25°C. While supercooled liquid water has been found in rare instances at temperatures approaching -40°C, it is considered to be a minimal hazard because liquid water contents are very small at these extremely cold temperatures. The algorithm then combines the cloud type information with the vertical temperature profiles to provide a vertical cross section along the satellite track where icing conditions are possible.

Table 1. Temperature ranges associated with supercooled liquid water for the different cloud types available from the CloudSat cloud classification algorithm.

Cloud types	Temperature range for icing
Sc, St	0°C to -10°C
Ac, As	0°C to -20°C
Cu, Ns, deep convective	0°C to -25°C
Ci, Cs, Cc	No icing

Figure 1 from Geerts (1998; adapted from Politovich (1996)) illustrates the relative frequency of supercooled liquid water content as a function of temperature for data collected by a research aircraft. Higher liquid water content is seemingly confined to temperatures warmer than about -14°C. Additionally, PIREPs of icing conditions were studied by Politovich (1996) and characterized by temperature (Fig. 2). Virtually all reports of icing were found at temperatures greater than -30°C.

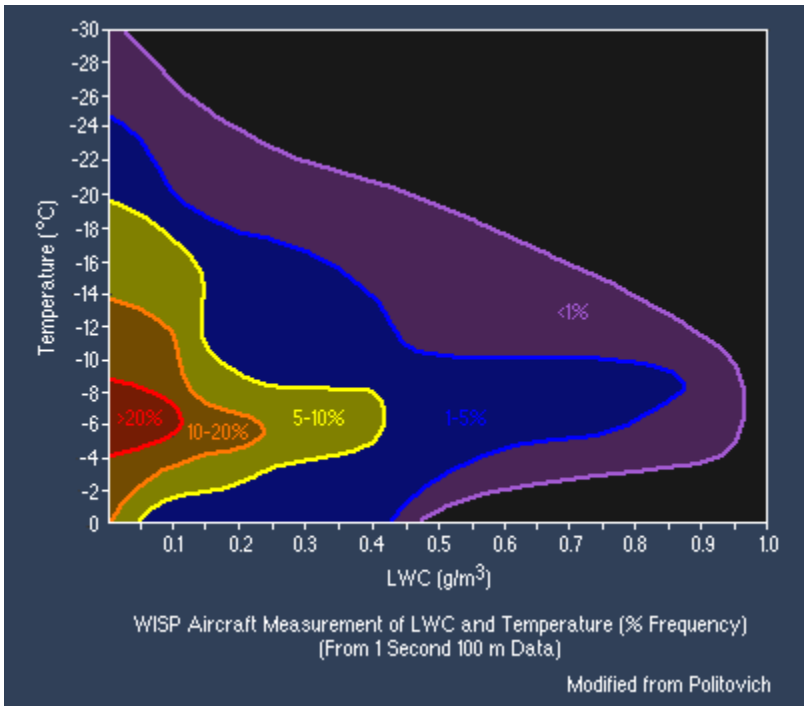

Fig. 1. Relative frequency of liquid water content found by a research aircraft as a function of temperature from Geert (1998; adapted from Politovich (1996)). Note that the higher frequencies are confined to relatively warm temperatures.

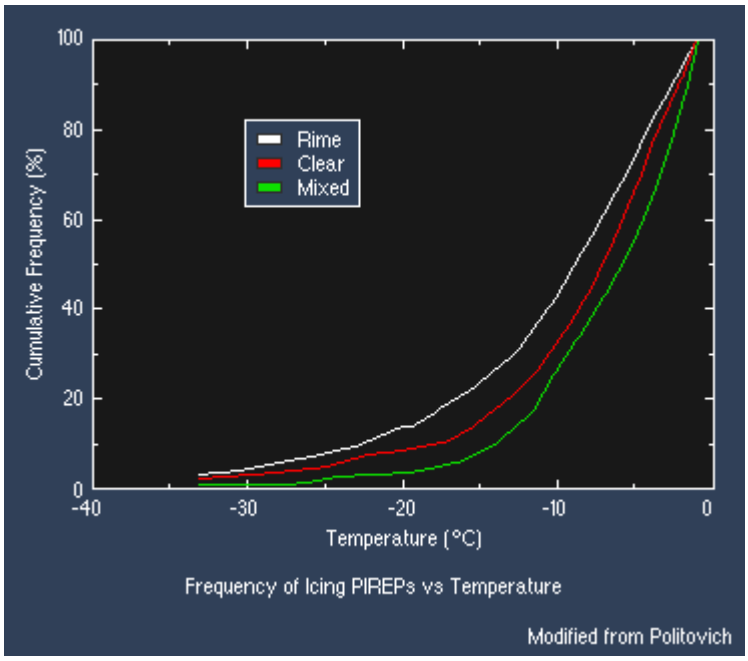

Fig. 2. Cumulative distribution function of PIREP reports as a function of temperature for rime, clear, and mixed icing conditions from Geert (1998; adapted from Politovich (1996)). Note the negligible number of reports at temperatures below -25°C.

It is important to note that our algorithm only states where icing conditions have the *potential* to exist rather than stating exactly where within the clouds exactly the icing does or does not exist. We use the CloudSat data to identify the cloud locations, which it is able to do very well. The existing CloudSat products do not allow us to easily gain additional insight into what parts of the clouds actually contain icing. For our purposes, identifying the potential for icing, which is important from an aviation safety perspective, is sufficient. Therefore our algorithm should be considered as a biased representation of icing conditions in the atmosphere. In the absence of a true measure of icing conditions the amount of bias cannot be known but as will be shown in Section 4, CLIP performs very well compared to CIP which is considered the state-of-the-art operational diagnosis of icing conditions over the continental United States.

4. INTERCOMPARISON OF CLIP AND CIP

Our interest in a global diagnosis of icing stems from a need to verify global icing forecasts. Since we cannot assess the performance of CLIP in a global domain, we instead will intercompare it against CIP over the data rich region of the continental U.S. The intercomparison was performed for the period 1 November 2007 through 31 January 2008. The approach taken was to find the closest-in-time CIP product to the entrance time of the satellite path into the CIP domain (the CIP domain is the same used as the 20 km Rapid Update Cycle (RUC) model). Maximum time differences between the hourly CIP product and a satellite track are always 30 minutes or less. Once the products were time matched, the CIP

data were interpolated to the satellite path to create a field that matches the CLIP product. CIP data was considered a 'yes' forecast if the probability of icing was greater than zero, regardless of intensity. At this point the CIP data is oversampled since its native resolution is 20 km and the satellite profiles occur every 1.1 km. The cross-sections (both CIP and CLIP) are degraded to 20 km horizontal resolution (18 profiles per coarse output profile) using the rule that if any profile indicates icing conditions at a particular vertical level then the profile is set to indicate icing. This process is repeated at all vertical levels; the vertical verifying resolution is 305 m (1000 ft). The matched grids (vertical cross-sections along the satellite path) can now be assessed.

For our analysis, we chose to use a simple neighborhood-based verification approach (Ebert 2008). The horizontal neighborhood is set to ± 2 grid boxes (40 km) while the vertical neighborhood is defined as ± 3 grid boxes (914 m). Further, the primary altitude range for intercomparison was chosen to be 10,000 ft to 20,000 ft (3048 m to 6096 m). These choices, combined with the unavoidable time differences between the satellite passes and CIP production, reflect the context in which the algorithm was developed and intended to be used; namely to assess forecasts of hazardous icing conditions at relatively low altitudes and at lead times approaching 24 hours. We err on the side of caution in choosing to use the somewhat liberal neighborhoods because of our aircraft safety concerns.

The dichotomous CIP and CLIP grids (cross-sections) were then verified using the neighborhood approach outlined above. In traditional settings, no additional information is present, and the results are tabulated into a 2x2 contingency table and scalar measures of performance are computed. However, in this setting additional information concerning the observed cloud temperatures is available. The cloud temperature information can be used to expand the 'non-event' cells (where CLIP diagnoses no icing) into counts where there is no cloud present, where there is cloud present but it is too warm for icing, or where there is cloud present but the algorithm says it is too cold for icing to occur. This concept is illustrated in Table 2. The traditional 2x2 table can be formed by combining the three non-event columns together to get the overall 'no icing observed' cells.

Table 2. Example contingency table that can be populated for the CLIP-CIP intercomparison. To arrive at the traditional 2x2 table, the b,c, and d cells are combined to form a ' CIP-yes, CLIP-no' cell while the f,g, and h cells are combined to form the 'CIP-no, CLIP-no' cell.

		CLIP			
		Yes	No, No Cloud	No, Warm Cloud	No, Cold Cloud
CIP	Yes	a	b	c	d
	No	e	f	g	h

The results were stratified into two groups, a non-convective group (St, Sc, As and Ac) and a convective group (Ns, Cu and deep convection) based upon the CloudSat cloud type. The results for the non-convective clouds are presented in Table 3. Significant agreement between CIP and CLIP is immediately evident. The bias (defined as CIP area / CLIP area) is equal to 1.2. The probability of detection (a/a+e in Table 2) is 0.7. In other words, 70% of the time when CLIP said icing was possible, CIP agreed with it. Further, when CIP indicates no icing, the dominant condition in CLIP is no cloud present. That the number of times CIP diagnosed icing while CLIP indicated conditions too warm for icing is fairly large may signal the presence a warm bias in the reanalysis temperature field. Additional work is planned to

assess differences in the temperature fields derived from the reanalysis data and the RUC 20 km data which is used as the background temperature field in CIP. It is not immediately evident what other situation may promote the observed behavior. Despite the fact that CIP was designed for non-convective situations (ie., conditions outside of deep convection), the relative performance differences between CLIP and CIP mimic those seen for non-convective cloud types (Table 4). Also analyzed but not shown was an additional stratification of oceanic versus continental profiles. Nearly identical performance was noted between the two regions. Therefore, we believe that these results illustrate that our CloudSat-derived icing diagnosis performs reasonably well when compared to CIP and by extension, may be suitable for us globally.

Table 3. Contingency table for non-convective clouds for the period 1 November 2007 to 31 January 2008 for the layer from 10,000 ft to 20,000 MSL.

		CLIP			
		Yes	No,No Cloud	No, Warm Cloud	No, Cold Cloud
CIP	Yes	37708	23217	4114	1003
	No	16132	336367	6101	6789

Table 4. As in Table 3 except for convective clouds.

		CLIP			
		Yes	No, No Cloud	No, Warm Cloud	No, Cold Cloud
CIP	Yes	46228	23217	5736	308
	No	9248	336367	3553	1766

5. CASE STUDIES OF CLIP COMPARED TO PIREPS

In this section, a small selection of events will be shown that illustrate the relation of CLIP to neighboring PIREPs. Three cases were selected from the winter season (November, December, and January) of 2007-2008 to illustrate the behavior of the CLIP algorithm. Case 1 is from 23 December 2007 when CloudSat passed through the west coast of the U.S. (Fig. 3). A frontal cloud system associated with a landfalling extratropical cyclone covers a portion of Washington and Oregon (Fig. 3a). CloudSat provided a detailed view of the vertical and horizontal structure of the frontal cloud (Fig. 3c). Case 2 from 13 December 2007 when CloudSat passes across the north-central U.S. (Fig. 4). The CloudSat track was on the west side of a comma-shaped midlatitude cyclone (Fig. 4a) and passed through the frontal band of clouds. Figure 5 shows the third case from 10 January 2008 where our focus is over the Great Lakes region. Marginal low-level clouds can be identified on Fig. 5a. However, for the region of interest, shown in Fig. 5c, the vertical cross section does show deeper clouds on the north side of segment 20, and very thin and low clouds on the south side.

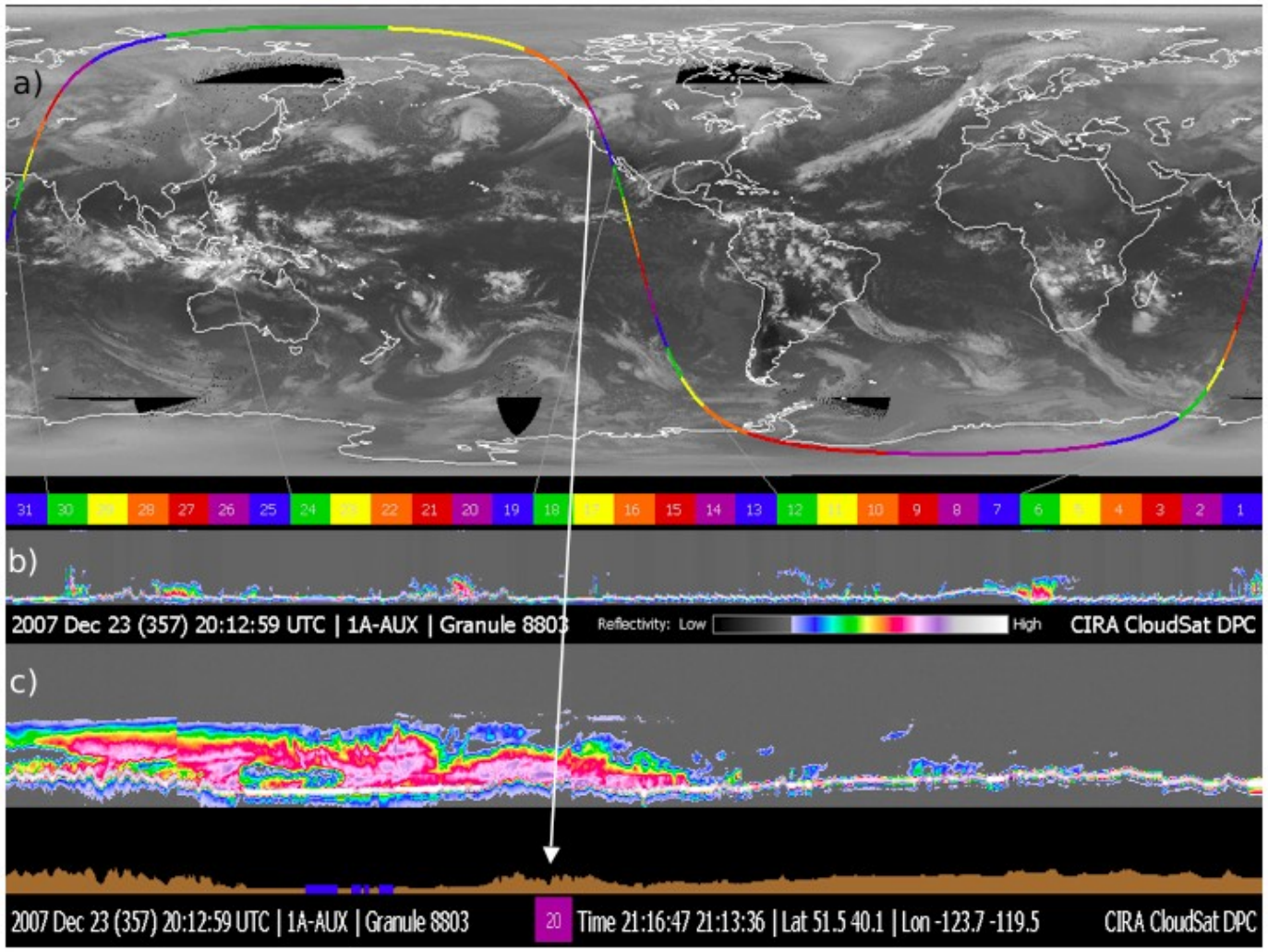

Fig. 3. CloudSat path on 23 December 2007 for Granule 88003. Region of intest is segment 20, shown in purple in panel a) over the pacific northwest of the United States. Panel b) shows reflectivity along entire path while panel c) shows reflectivity for segment 20 alone and illustrates the rich plume of clouds well. North is on the left side of panel c) and south is on the right.

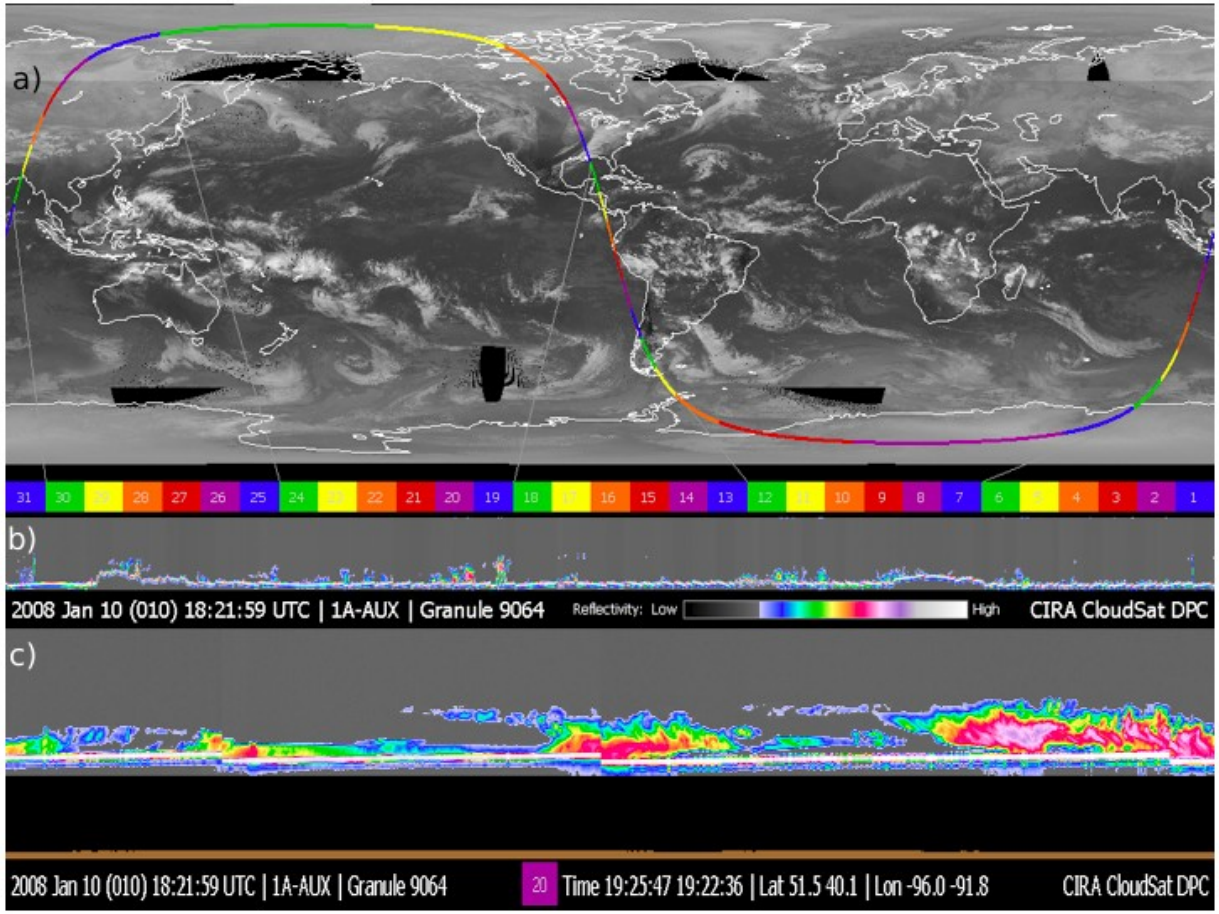

Fig. 4. As in Fig. 3 except for Granule 9064 on 10 January 2008. The highlighted segment is number 20.

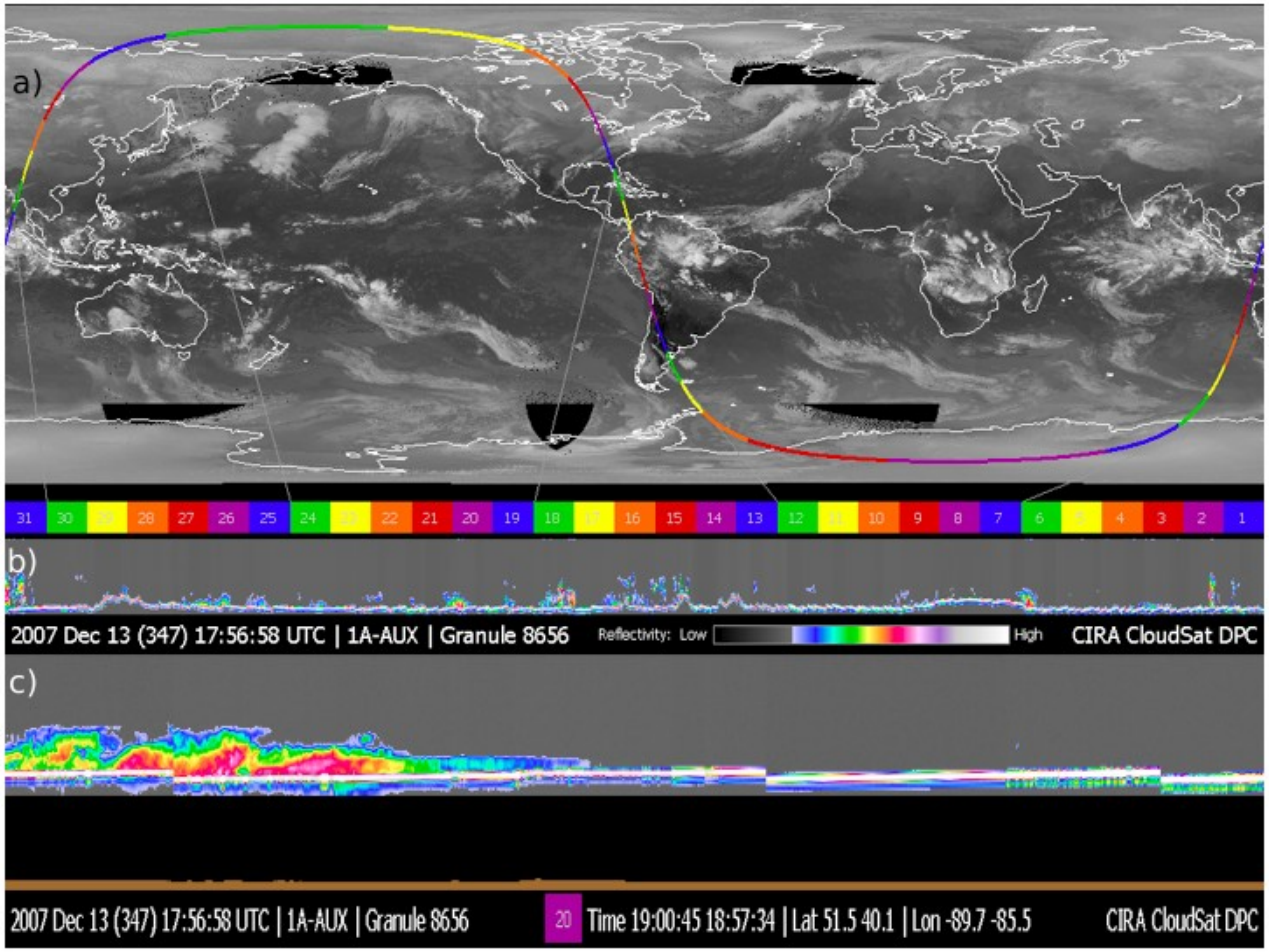

Fig. 5.As in Fig. 3 except for Granule 8656 on 13 December 2007. The highlighted segment is number 20.

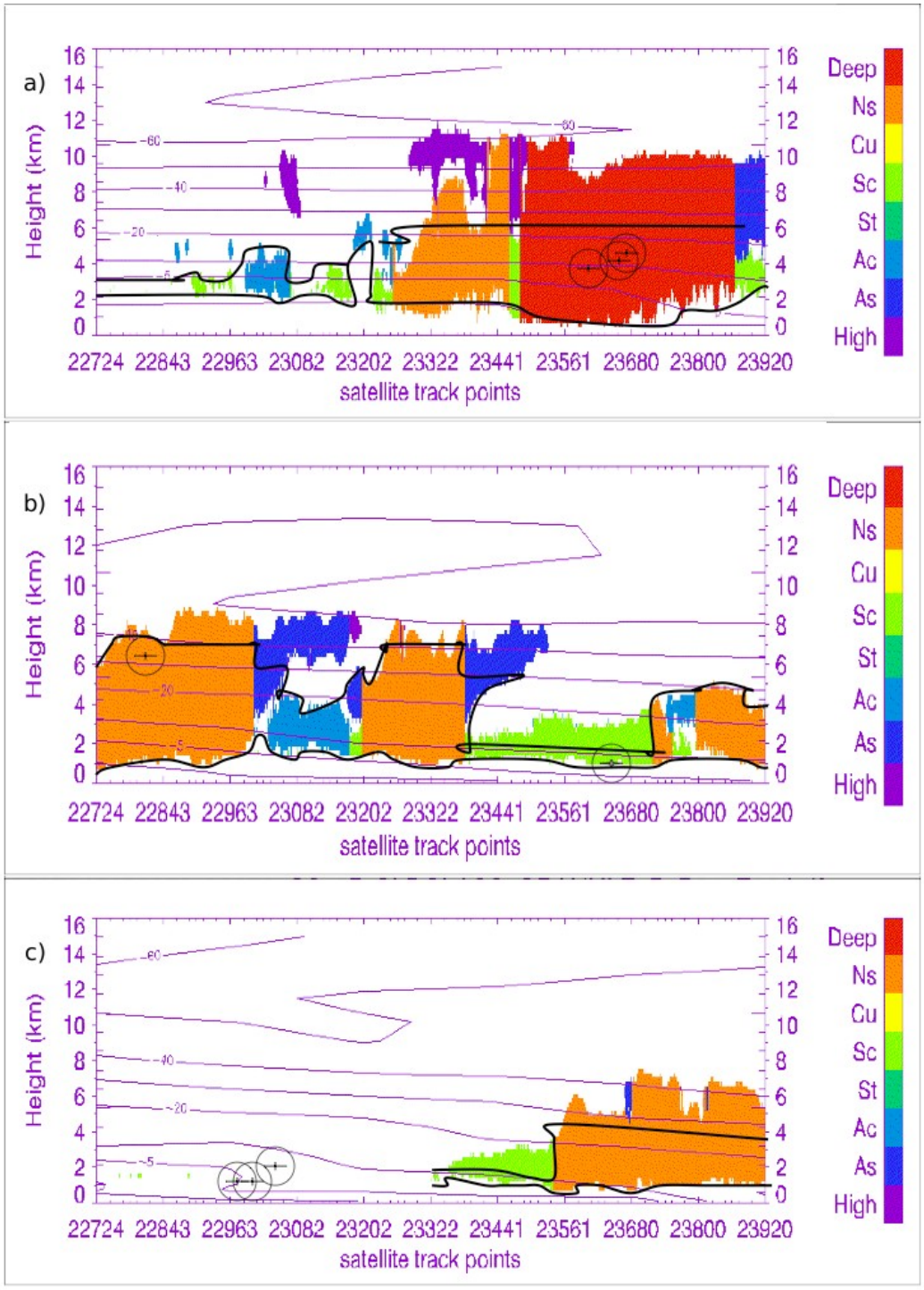

Fig. 6. Vertical cross-sections of cloud type along the CloudSat track for segment 20 for cases a) 23 December 2007, b) 10 January 2008 and c) 13 December 2007. Heavy black line on each plot represents bounds of icing region indicated by CLIP algorithm. Plus symbols surrounding by open circles indicate PIREP locations.

For each of these cases, we found PIREPs that were close in space and time to the satellite track. For the 23 December 2007 and 10 January 2008 cases, three PIREPs were identified per case while two PIREPs were available for the 13 December 2008 case. Vertical cross-sections of the regions of interest identified in Figs. 3, 4, and 5 are shown in Fig. 6. For the 23 December 2007 and 10 January 2008 cases, where deep, moist clouds intersected the satellite path, good agreement is evident between CLIP and PIREPs. For the 13 December 2007 case, where the atmosphere was much drier, the PIREPs appear in a region dominated by sparse, shallow stratocumulus. Perhaps due to temporal differences and the sparse nature of the cloud deck, the CLIP algorithm did not identify cloud features at the exact PIREP locations.

6. SUMMARY

An algorithm to detect cloud icing conditions using CloudSat information has been developed. By combining CloudSat cloud classification information with a temperature data from a global model, a high-resolution global, polar orbiting diagnosis of icing that may be used for a variety of purposes. We intend to use the diagnosis as the observation field to verify global forecasts of icing hazard used for aviation. Such a view of global icing conditions is unavailable elsewhere. The algorithm was shown to perform well against the current state of the art operational icing diagnosis in the U.S., CIP. Additionally, several brief case studies showed a good agreement to pilot reports of icing conditions.

ACKNOWLEDGMENTS

We would like to acknowledge the NASA CloudSat project for making CloudSat data availiable to the scientific community. Paul Hamer of NOAA/ESRL/GSD was instrumental in making the global reanalysis data available to us in a timely manner.

7. REFERENCES

Bernstein, B.C., McDonough, F., Politovich, M.P., Brown, B.G., Ratvasky, T.P., Miller, D.R., Wolff, C.A., and Cunning, G.C., 2005: Current Icing Potential (CIP): Algorithm description and comparison with aircraft observations. *J. Applied Meteor.*, **44**, 969 – 986.

Curry, J.A., and G. Liu, 1992: Assessment of aircraft icing potential using satellite observations. *J. Applied Meteor.*, **31**, 605 – 621.

Ebert, E.E., *2008*: *Fuzzy* verification of high resolution gridded forecasts: A review and proposed framework. *Meteorol. Appls.*, **15**, 51-64.

Ellrod, G.P., 1996: The use of GOES-8 multi-spectral imagery for the detection of aircraft icing regions. Preprints, 8th Conf. on Satellite Meteor. and Ocean., Amer. Meteor. Soc., Atlanta, GA, 168-171.

Ellrod, G.P., and A.A. Bailey, 2007: Assessment of Aircraft Icing Potential and Maximum Icing Altitude from Geostationary Meteorological Satellite Data. *Wea. Forecasting*, **22**, 160–174.

Geerts, B., 1998: Supercooled liquid water and airframe icing. Retrieved from http://www-das.uwyo.edu/~geerts/cwx/notes/chap08/supercooled.html.

Heymsfield, A.J., and L.M. Miloshevich, 1989: Evaluation of liquid water measuring instruments in cold clouds sampled during FIRE. *J. Atmos. Ocean. Tech.*, **6**, 378-388.

Heymsfield, A.J., and L.M. Miloshevich, 1993: Homogeneous ice nucleation and supercooled liquid water in orographic wave clouds. *J. Atmos. Sci.*, **50**, 2335-2353.

Lee, T.F., F.J. Turk, and K. Richardson, 1997: Stratus and fog products using GOES-8-9 3.9 μm data. *Wea. Forecasting*, **12**, 664–677.

Minnis, P., L. Nguyen, W.L. Smith, Jr., M.M. Khaiyer,

R. Palikonda, D.A. Spangenberg, D.R. Doelling, D. Phan, G.D. Nowicki, P.W. Heck, and C.A. Wolff, 2004: Real-time cloud, radiation, and aircraft icing parameters from GOES over the USA. Preprints, 13th Conf. on Satellite Meteor. and Ocean., Amer. Meteor. Soc., Norfolk, VA, CD-ROM, P7.1.

Politovich, M.P., 1996: Response of a research aircraft to icing and evaluation of severity indices. *Journal of Aircraft*, **33**, 291-297.

Rauber, R.M., and A. Tokey, 1991: An explanation for the existence of supercooled water at the top of cold clouds. *J. Atmos. Sci.*, **48**, 1005-1023.

Rosenfeld, D., and W.L. Woodley, 2000: Deep convective clouds with sustained supercooled liqid water down to -37.5℃. *Nature*, **405**, 440-442.

Smith, W.L., Jr., P. Minnis, and D.F. Young, 2000: An icing product derived from operational satellite data. Preprints, 9th Conf. on Aviation, Range and Aerospace Meteorology, Amer. Meteor. Soc., Orlando, FL, 256-259.

Stephens, G.L., D.G. Vane, R.J. Boain, G.G. Mace, K. Sassen, Z. Wang, A.J. Illingworth, E.J. O'Connor, W.B. Rossow, S.L. Durden, S.D. Miller, R.T. Austin, A. Benedetti, C. Mitrescu, and The CloudSat Science Team: 2002, The CLOUDSAT Mission and the A-Train. *Bull. Amer. Met. Soc.*, **83**, 1771-1790.

Tabazadeh, A., Y.S. Djikaev, and H. Reiss, 2002: Surface crystallization of supercooled water in clouds. *PNAS*, **99**, 15873-15878.

Thompson G., R. Bullock, and T.F. Lee, 1997: Using satellite data to reduce spatial extent of diagnosed icing. *Wea. Forecasting*, **12**, 185–190.

Vivekanandan, J., G. Thompson, and T.F. Lee, 1996: Aircraft icing detection using satellite data and weather forecast model results. Proc. Int. Conf. on Aircraft Icing, Vol. II, Springfield, VA, Federal Aviation Administration, 365-373.

Wolff, C.A., T.F. Lee, C. Mitrescu, S. Landolt, and S.D. Miller, 2008: Using CloudSat data to validate icing products. Preprints, 13th Conf. on Aviation, Range and Aerospace Meteorology, Amer. Meteor. Soc., New Orleans, LA, P4.11.